Computational Screening of Porous Metal-Organic Frameworks and Zeolites for the Removal of SO_2 and NO_x from Flue Gases

Weizhen Sun
State-Key Laboratory of Chemical Engineering, East China University of Science and Technology, Shanghai 200237, China

Dept. of Chemical and Biomolecular Engineering, University of California, Berkeley, CA 94720

Key Laboratory of Advanced Control and Optimization for Chemical Processes, East China University of Science and Technology, Shanghai 200237, China

Li-Chiang Lin
Dept. of Chemical and Biomolecular Engineering, University of California, Berkeley, CA 94720

Xuan Peng
Dept. of Chemical and Biomolecular Engineering, University of California, Berkeley, CA 94720

Dept. of Automation, College of Information Science and Technology, Beijing University of Chemical Technology, Beijing 100029, China

Berend Smit
Dept. of Chemical and Biomolecular Engineering, University of California, Berkeley, CA 94720

Dept. of Chemistry, University of California, Berkeley, CA 94720

Materials Sciences Div., Lawrence Berkeley National Laboratory, Berkeley, CA 94720

DOI 10.1002/aic.14467
Published online April 23, 2014 in Wiley Online Library (wileyonlinelibrary.com)

Sulfur oxides (SO_2) and nitrogen oxides (NO_x) are principal pollutants in the atmosphere due to their harmful impact on human health and environment. We use molecular simulations to study different adsorbents to remove SO_2 and NO_x from flue gases. Twelve representative porous materials were selected as possible candidates, including metal-organic frameworks, zeolitic imidazolate frameworks, and all-silica zeolites. Grand canonical Monte Carlo simulations were performed to predict the (mixture) adsorption isotherms to evaluate these selected materials. Both Cu-BTC and MIL-47 were identified to perform best for the removal of SO_2 from the flue gases mixture. For the removal of NO_x, Cu-BTC was shown to be the best adsorbent. Additionally, concerning the simultaneous removal of SO_2, NO_x, and CO_2, Mg-MOF-74 gave the best performance. The results and insights obtained may be helpful to the adsorbents selection in the separation of SO_2 and NO_x and carbon capture. © 2014 American Institute of Chemical Engineers *AIChE J*, 60: 2314–2323, 2014

Keywords: adsorbent material, harmful gas removal, adsorption separation, molecular simulation

Introduction

Under the Clean Air Act, the U.S. Environmental Protection Agency is required to set National Ambient Air Quality Standards (NAAQS) for pollutants harmful to public health and the environment.[1] Based on this NAAQS, six principal air pollutants were identified, including particulate matter, ground level ozone, carbon monoxide, sulfur oxides (SO_2), nitrogen oxides (NO_x), and lead. Among them, a portion of particulate matter is formed in the air when gases such as SO_2 and NO_x are transformed by chemical reactions. The ground level ozone is created by chemical reactions between NO_x and volatile organic compounds in the presence of sunlight. It is clear that besides their direct significant impacts on human health and environment, both SO_2 and NO_x also exert more negative effects by forming other air pollutants.

These two most harmful air pollutants are emitted into the atmosphere mainly through automobile exhaust gases and industrial flue gases.[2] For example, in China 87% of SO_2 and 67% of NO_x come from coal-fired combustion.[3] A typical composition of untreated flue gases from coal-fired plants burning low-sulfur coal is as follows (by volume): N_2 (70–75%), CO_2 (15–16%), O_2 (3–4%), water vapor (5–7%), SO_2

Additional Supporting Information may be found in the online version of this article.

Correspondence concerning this article should be addressed to B. Smit at berend-smit@berkeley.edu.

(800 ppm), NO_x (500 ppm), and traces of other species.[4,5] For burning high-sulfur coals, the content of SO_2 may reach 2000 ppm.[6] Accordingly, it is absolutely necessary to remove them efficiently from flue gases before their emission into the atmosphere. Till now, a variety of methods have been developed to remove these two harmful gases from flue gases. The wet flue-gas desulfurization is one of common technologies used to remove SO_2 from exhaust flue gases. The method uses a slurry of alkaline sorbent, usually limestone or lime and so on.[7] Selective catalytic reduction (SCR) is a means of converting NO_x into N_2 and water in the presence of catalyst.[8] Additionally, the SNOX technology of Haldor Topsoe combined the wet-gas sulfuric-acid process and SCR process for the simultaneous removal of SO_2 and NO_x.[2]

Adsorption can be a promising alternative to the aforementioned technologies to remove SO_2 due to its unique advantages such as small energy requirement for the adsorbent regeneration, relatively simple adsorber design, and less problems in waste disposal.[9] In the literature,[9] an adsorption process using silicalite, an hydrophobic molecular sieve, was put forward for the removal of SO_2 from combustion gases. Some studies focused on the simultaneous adsorption of SO_2 and NO_x from flue gases using porous γ-Al_2O_3 supported sodium or sodium carbonate as sorbents.[2,10] In addition, some type of activated carbon derived from a petroleum pitch impregnated with certain iron derivatives showed good SO_2 and NO_x adsorption characteristics.[11] The adsorption performance of 5A and 13X zeolites was also investigated experimentally for adsorbing SO_2, NO, and CO_2.[12]

As a new emerging class of porous materials, metal-organic frameworks (MOFs) have attracted extensive research interests for their potential applications in clean energy applications. These materials are promising adsorbents due to their high surface areas, tunable pore size, and adjustable internal surface properties.[13] In the past few years, many studies in the literature have been focused on the investigation and screening of MOFs for the separation of CO_2 from flue gases for carbon capture and storage.[5,14–17] These MOFs might also be promising materials for the removal of SO_2 and NO_x.[18–22]

Because of the huge number of available porous adsorbents, it is crucial to identify the characteristics of those materials that have a high adsorption uptake and selectivity for the removal of SO_2 and NO_x. Molecular simulations have been proved to be a powerful way to effectively investigate and evaluate porous materials' adsorption performance.[14,23] Most of these simulation studies were focused on carbon capture, and far less attention has been paid to the removals of SO_2 and NO_x. One recent publication reported computional screening of porous materials, such as carbons, zeolites, and MOFs for desulfurication of flue gases.[6] In this study, the seperation condition was set at the pressure of 4 MPa, whereas practical flues gas condition is 0.1 MPa. Additionally, NO_x removal was not considered in Ref. 6.

In the present work, we study gaseous adsorption properties in 12 selected porous materials, and these include six MOFs, two zeolitic imidazolate frameworks (ZIFs), and four zeolites. These MOFs and ZIFs differ in organic linker, metal cluster, and topology. Their structures are shown in Figure 1 and their pore shape and pore volume are listed in Table 1. Among them, Cu-BTC, Mg-MOF-74, and Zn-MOF-74 possess open-metal sites, which have been proven as promising materials for carbon capture.[25] The zeolites we have selected here fall into two groups: those with cages separated by windows (LTA, FAU, DDR) and those with intersecting channels (MFI). It should be noted that some materials in Ref. 6 are not studied in our current work, especially cation-exchanged zeolites due to two primary considerations. First, due to the lack of experimental measurements and accurate force fields, the predictions made by the use of generic force field for those materials might involve large uncertainties. Second, Peng and Cao[6] have also found that Na-5A and Na-13X can be the most promising materials for the removal of sulfide from the CH_4—CO_2—H_2S and N_2—CO_2—SO_2 mixtures. However, these zeolites were excluded eventually as they cannot be easily regenerated even at high temperature due to the strong adsorbent–adsorbate interactions. In other words, it could be energy-intensive to use these cation-exchanged zeolites for the considered separations.

In this work, we use the following gas mixture to mimic the real post combustion flue gas (volume fraction): N_2 (0.7975), CO_2 (0.15), O_2 (0.05), SO_2 (0.002), NO_2 (250ppm), and NO (250ppm). The pressure condition adopted in this work covers 1 bar, which is exactly the operation condition of industrial flue gas. The force fields of eight materials used in our work were verified by comparing to experimental measurements reported in the literature. In particular, the force-field parameters of Mg-MOF-74 was adjusted based on density function theory (DFT) calculations, and the resulting force field can reproduce the experimentally measured CO_2 isotherm data. Water was neglected given that we assumed the flue gases could be dried. We study the most used screening criteria, which includes the absolute adsorption q_i, the adsorption selectivity S_{ads}, and the working capacity Δq_i.

Models and Simulation Details

Material structure

In this work, we consider the all-silica zeolites LTA, FAU, MFI, and DDR. The structures used in our work are the ones fully optimized with DLS-76 which are obtained from the IZA database.[26] The detailed crystal structure parameters of the aforementioned zeolites and MOFs are summarized in Table 1, and their structures are shown in Figure 1.

As mentioned before these zeolites fall into two categories: (a) cages separated by windows (LTA, FAU, and DDR) and (b) intersecting channels (MFI). The LTA zeolite has a sodalite cage of about 10 Å in diameter with 24 Si atoms as zero-dimensional periodic building unit. The narrow windows of about 4 Å in diameter connect these almost spherical cages. The periodic building unit of FAU is two-dimensional, in which the β-cages are linked through double six-rings of about 7.4 Å in diameter into the hexagonal faujasite layer. The trigonal DDR has 12-rings double cups consisting of 30 Si atoms. The connection of Si30-units through the Si2-dimers generates [5^{12}]-cages in the layer, which reveal two types of nest-like recesses: Site A with the six-ring and Site B (Site C) where [5^{12}]-cages share faces. These cages with the size of 277.8 Å^3 are separated by the 3.65 × 4.37 Å size windows. Based on the secondary building units (SBUs) of double five-ring, the MFI zeolite has intersecting straight and zigzag channels. The free diameter is 5.1 × 5.5 Å for zigzag channels and 5.3 × 5.6 Å for straight channels.[27]

For those structures of M-MOF-74 (M = Mg or Zn), we used the crystal structures optimized by DFT given from one

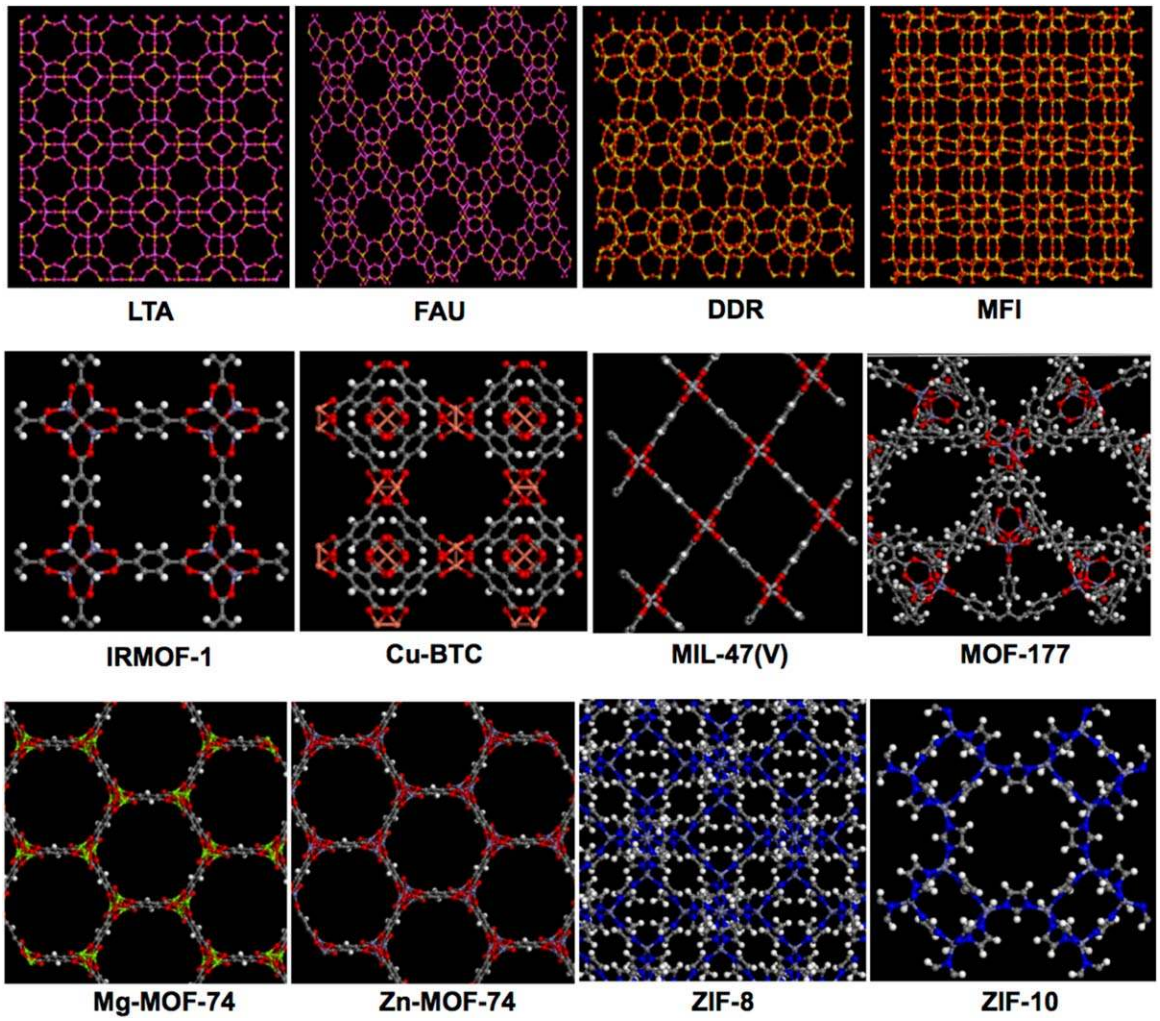

Figure 1. Atomic structure of materials studied in this work.

Materials are represented as balls and sticks. [Color figure can be viewed in the online issue, which is available at wileyonlinelibrary.com.]

of our previous works.[17] Dzubak et al. have shown that simulated adsorption properties are very sensitive to the adopted crystal structures for these materials, and the crystal structure of Mg-MOF-74 obtained from powder diffraction is not sufficiently accurate. For the rest of MOFs, we used the crystal structures obtained from experimental XRD data. IRMOF-1 is one of the most widely studied MOFs. IRMOF-1 consists of an oxide-centered Zn_4O tetrahedron edge-bridged by six carboxylates to give the octahedron-shaped SBU, forming a regular and three-dimensional (3-D) lattice of cubic cavities of about 10.9 or 14.3 Å in diameter.[28] The MOF Cu-BTC has 12 carboxylate oxygen atoms from two BTC (benzene-1,3,5-tricarboxylate) ligands which bind to four coordination sites for each of the three Cu^{2+} ions.[29] Its structure has main

Table 1. Structural Properties for the Materials Considered in This Work

Materials	Unit Cell (Å) *a*/*b*/*c*	Cell Angle (°) $\alpha/\beta/\gamma$	Pore Shape and Size in Diameter (Å)	Pore Volume (cm^3/g)
LTA	24.56/24.56/24.56	90/90/90	Cage/window, 10.0/4.0	0.31[a]
FAU	24.28/24.28/24.28	90/90/90	Cage/window, 11.2/7.4	0.328[a]
DDR	13.86/13.86/40.89	90/90/120	Cage/window, 7.7/3.7	0.139[a]
MFI	20.02/19.90/13.38	90/90/90	Intersecting channel, 5.1-5.5/5.3-5.6	0.165[a]
IRMOF-1	25.83/25.83/25.83	90/90/90	Cubic, 10.9/14.3	1.369[a]
Cu-BTC	26.34/26.34/26.34	90/90/90	Pocket/channel, 5.0/9.0	0.863[a]
MIL-47(V)	6.81/16.12/13.92	90/90/90	Channel, 11.0	0.606[a]
MOF-177	37.07/37.07/30.03	90/90/120	Channel, 10.8	1.968[a]
Mg-MOF-74	26.11/26.11/6.92	90/90/120	Channel, 15	0.782[a]
Zn-MOF-74	26.10/26.10/6.88	90/90/120	Channel, 10.3	0.54[b]
ZIF-8	16.99/16.99/16.99	90/90/90	Cage/window, 11.6/3.4	0.663[c]
ZIF-10	27.06/27.06/19.04	90/90/90	Cage/window, 12.1/8.2	0.689[c]

[a]From the work of Krishna and van Baten.[14]
[b]From the work of Peng and Cao.[6]
[c]From the work of Park et al.[24]

Table 2. Molecular Models of Guest Molecules Considered in This Work

Species	Geometry	Site	σ (Å)	ε/k_B (K)	q (e)	Reference
CO_2*	$d_{CO} = 1.16$ Å	C	2.80	27.0	0.7	36
		O	3.05	79.0	−0.35	
N_2*	$d_{NN} = 1.10$ Å	N	3.31	36.0	−0.482	36
		COM	0	0	0.964	
O_2	$d_{OO} = 1.21$ Å	O	3.05	54.4	−0.112	37
		COM	0	0	0.224	
SO_2	$d_{SO} = 1.43$ Å	S	3.62	145.9	0.4710	38
	∠OSO = 119.5°	O	3.01	57.4	−0.2355	
NO_2	$d_{NO} = 1.20$ Å	N	3.24	50.36	0.146	39
	∠ONO = 134.3°	O	2.93	62.51	−0.073	
NO	$d_{NO} = 1.15$ Å	N	3.014	79.5	0.0288	40
		O	2.875	96.94	−0.0288	

*For the simulations of CO_2 and N_2 adsorbed in all-silica zeolites, their force-field parameters are different and they are taken from ref. 41.

channels of a square cross section of about 9 Å in diameter and tetrahedral side pockets of about 5 Å in diameter, which are connected to the main channels by triangular windows of about 3.5 Å in diameter.[30] MIL-47(V) has a 3-D orthorhombic structure, with large pores in the [100] direction. Based on the van der Waals radii, the free diameter of these pores is 10.5 × 11.0 Å.[31] Four walls of benzyl units and four chains of corner-shared vanadium octahedra delimit each tunnel. The topology of MOF-177 is a coordinated net, in which the center of the octahedral $OZn_4(CO_2)_6$ cluster acts as the site of six coordination, and as well as the center of the BTB (1,3,5-benzene-tribenzoate) unit as the site of three coordination.[32] In the structure of M-MOF-74 (M = Mg, Zn), helical M—O—C rods of composition $[O_2M_2](CO_2)_2$ are constructed from 6-coordinated M(II) centers.[33] The rods are linked by the benzene units of the DOBDC (2,5-dihydroxybenzenedicarboxylate) to produce parallel rod packing and hexagonal one-dimensional channels with pore opening that has a diameter of about 15 Å.[33,34] The ZIF crystal structures are based on the nets of zeolites, in which tetrahedral Si(Al) and the bridging O are replaced by transition metal such as Zn(II) or Co(II) and imidazolate-type linker, respectively.[24] For example, ZIF-8 has the zeolite topology SOD possessing large pores of 11.6 Å connected through small apertures of 3.4 Å; whereas for ZIF-10 with the zeolite topology MER, the size of large pores is 12.1 Å connected by apertures of 8.2 Å.[35]

Force field

For the guest molecules, the interactions are described with point charges and Lennard-Jones interactions. The partial charges and Lennard-Jones parameters are taken from the literature. These parameters have been fit to the experimental bulk properties of guest such as the vapor–liquid equilibrium. The molecular geometry, Lennard-Jones potential parameters, and partial point charges of CO_2, N_2, O_2, SO_2, NO_2, and NO are summarized in Table 2. The TraPPE force field is used to model CO_2 and N_2.[36] In this model, the interactions of CO_2 are modeled with three-sites Lennard-Jones model and partial point charges are centered at each Lennard-Jones site to approximate the first-order electrostatic and second-order induction interactions. For N_2, each nitrogen atom is modeled by a Lennard-Jones site with atomic charge separated by the experimental bond length of 1.10 Å; a point charge of +0.964 e is placed at the center of mass (COM) of the N_2 molecule to maintain charge neutrality. Similarly, the O_2 molecule is represented as a rigid three-site model with two sites located at O atoms and the third one at its COM.[37] SO_2 is modeled as a three-site Lennard-Jones model and the partial point charges are centered at each atom.[38] Similar to SO_2, the NO_2 molecule is modeled as a three-site Lennard-Jones model with one charged interaction site located at each atom.[39] NO is modeled as a two-site Lennard-Jones model with partial charges assigned on each site.[40]

For the framework atoms the force fields for zeolites are taken from the literature.[41,42] The Lennard-Jones interaction parameters of the MOF and ZIF atoms are obtained from the UFF or DREIDING force fields, and the corresponding partial charges are based on DFT calculations (see Supporting Information Tables S1 through S9).[14,15,41,43–53] The Lorentz-Berthelot mixing rules are used to calculate the cross site-site Lennard-Jones parameters. For Mg-MOF-74, the commonly used force fields yield a poor prediction of the CO_2 adsorption isotherm.[14] To make reliable predictions, we used a simple, but effective, way to improve the force fields. The method adjusts the sigma parameter assigned on the metal center to ensure that the binding energy calculated by the force field reproduces the binding energy calculated from DFT calculations (Lee et al., Unpublished). We found that a 45% reduction of the UFF sigma parameter of Mg gave a good agreement with the DFT binding energy.

Grand canonical Monte Carlo (GCMC) simulations were performed to predict pure component and mixture isotherms for the flue gases in different zeolites and MOFs. In the grand canonical ensemble, the temperature, volume of the adsorbent system, and the chemical potentials of all the adsorbing species are specified.[54] The Peng–Robinson equation of state was used to convert the bulk pressures into corresponding chemical potentials. All framework atoms were held fixed. Periodic boundary conditions were applied in all three dimensions. Short-range interactions were truncated and shifted to zero at a cutoff radius of 12.0 and 12.8 Å for zeolites and MOFs, respectively. The simulation box was defined by at least twice this radius in all orthogonal directions, and no tail corrections were used.[17] The long-range electrostatic interaction energy was computed using the Ewald summation technique. To accelerate simulations, the framework-guest interaction energies were stored in a precomputed grid with a spacing of 0.15 Å. Trial configurations were generated by attempting random translation, rotation, regrowth (insertion and deletion), swap (insertion or deletion), and identity change moves (for mixture adsorption simulations).[55] It is well known that, some microporous frameworks may contain channels, pockets, or cages that are not accessible experimentally,[14] but can be accessed in a Monte Carlo simulation. To prevent the artificial adsorption of molecules, we have used the same blocking information as we used our previous

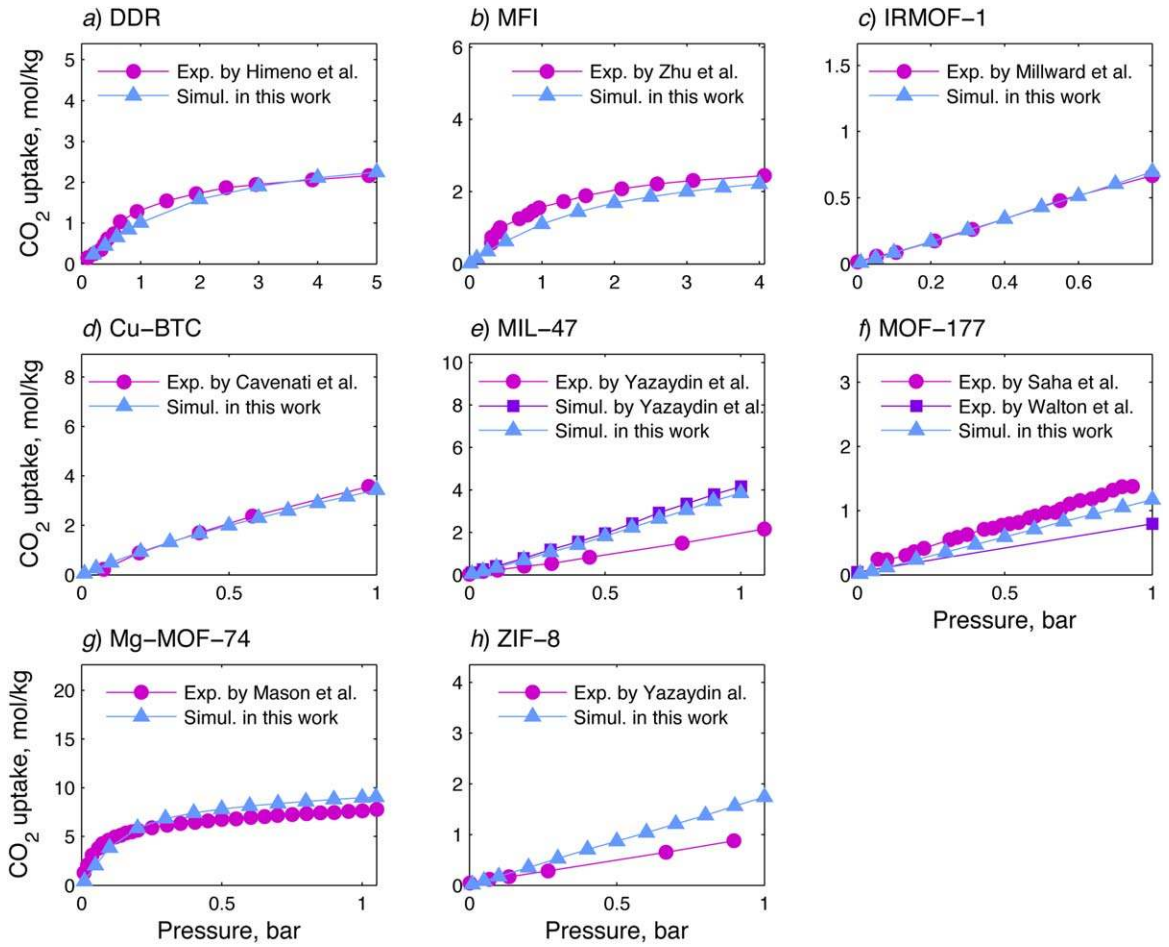

Figure 2. Comparison between our simulated pure CO_2 adsorption isotherms with (a) experimental data of Himeno et al.[60] in DDR at 298 K; (b) experimental data of Zhu et al.[59] in MFI at 303 K; (c) experimental data of Millward and Yaghi[58] in IRMOF-1at 298 K; (d) experimental data of Cavenati et al.[61] in Cu-BTC at 303 K; (e) experimental data of Yazaydin et al.[15] and simulated one of Yazaydin et al.[15] in MIL-47 at 298 K; (f) experimental data of Saha et al.[57] and Walton et al.[44] in MOF-177 at 298 K; (g) experimental data of Mason et al.[56] in Mg-MOF-74 at 298 K; (h) experimental data of Yazaydin et al.[15] in ZIF-8 at 298 K.

[Color figure can be viewed in the online issue, which is available at wileyonlinelibrary.com.]

work.[16] Note that, for simplification, we applied the blocking information of CO_2 molecules to all guest molecules considered in this work.

To evaluate adsorbents for practical application, many criteria have been put forward, but none of them is perfect. In this present work, three most used ones are adopted: absolute adsorption q_i, adsorption selectivity S_{ads}, and working capacity Δq_i. First, the absolute adsorption q_i at the mixture condition refers to the molar loading of the component i in equilibrium with bulk fluid phase of N_2—CO_2—O_2—SO_2—NO_2—NO at total pressure P and temperature T. Additionally, the adsorption selectivity S_i was defined by the following equation

$$S_i = \frac{q_i/\Sigma_{j\neq i} q_j}{p_i/\Sigma_{j\neq i} p_j} \tag{1}$$

where q_i is defined as above and p_i represents the partial pressure of component i in fluid phase; both i and j refer to the species N_2, CO_2, O_2, SO_2, NO_2, and NO in flue gases mixture. It should be noted that, in this work, we also considered a special scenario of utilizing these porous materials to remove SO_2, NO_x, and CO_2 simultaneously. CO_2 is one of the key contributors to global warming, and there is a necessity to reduce CO_2 emission into the atmosphere. For this simultaneous removal, the separation selectivity S_{snc} was defined as

$$S_{snc} = \frac{(q_{SO_2}+q_{NO_x}+q_{CO_2})/(q_{N_2}+q_{O_2})}{(p_{SO_2}+p_{NO_x}+p_{CO_2})/(p_{N_2}+p_{O_2})} \tag{2}$$

Finally, the working capacity Δq_i is defined as the difference in loading of component i between the adsorption ($q_{i,a}$) and desorption conditions ($q_{i,d}$)

$$\Delta q_i = q_{i,a} - q_{i,d} \tag{3}$$

Results and Discussion

Comparing of the simulated CO_2 isotherm with experimental data

To verify the validation of the molecule potentials adopted in this work, the simulated pure component CO_2 isotherms in different porous materials were compared with experiments data from the literature[15,44,56–61] and other simulation results[15]

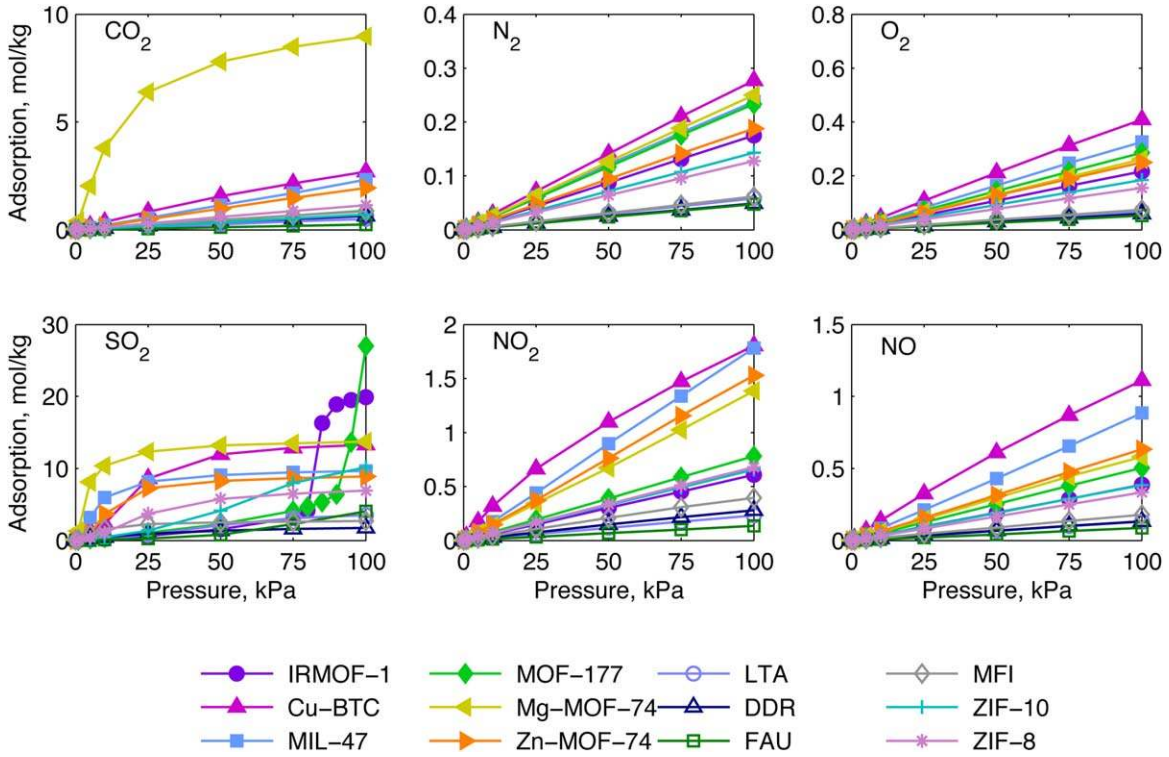

Figure 3. Simulated pure component isotherms for CO_2, N_2, O_2, SO_2, NO_2, and NO in 12 porous materials at 313 K.

[Color figure can be viewed in the online issue, which is available at wileyonlinelibrary.com.]

as illustrated in Figure 2. The result shows that the predicted isotherms given from the adopted force fields are generally in reasonable agreement with experimental data for all of these materials. There are, unfortunately, very limited experimental isotherms of SO_2, NO_2, and NO that are available to further validate the potential we have implemented in this work.

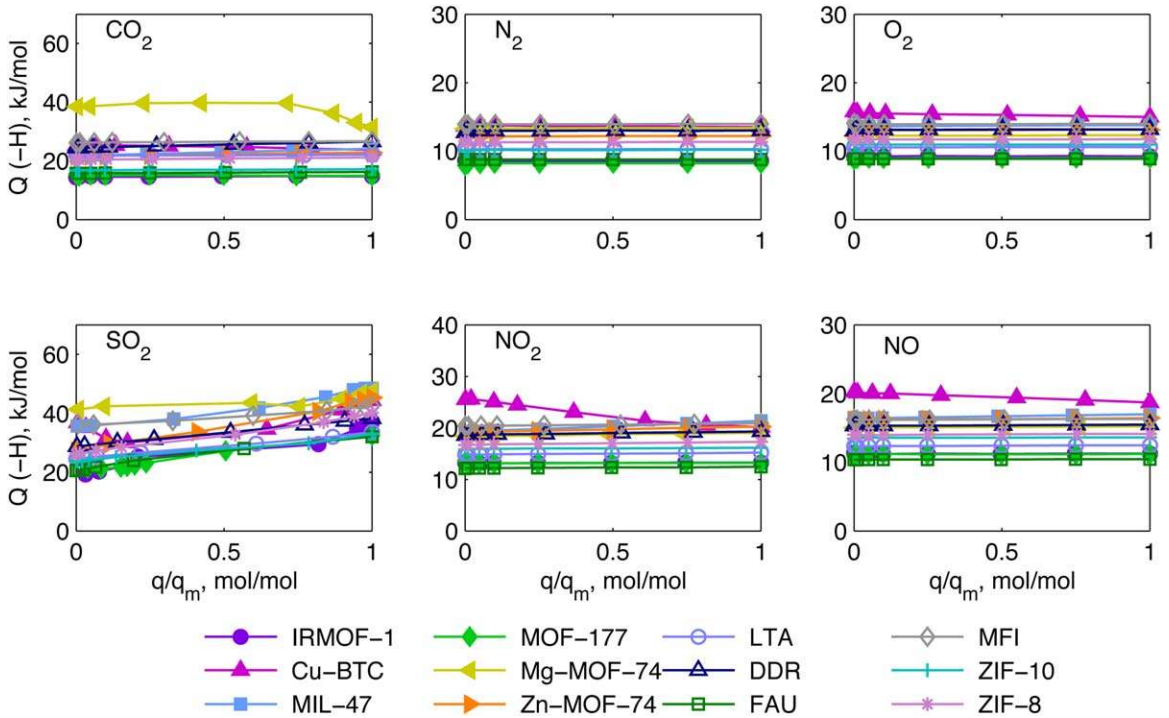

Figure 4. Simulated isosteric heat of adsorption of pure components for CO_2, N_2, O_2, SO_2, NO_2, and NO in 12 porous materials as a function of normalized loading (i.e., normalized by the corresponding loading at 1 bar) at 313 K.

[Color figure can be viewed in the online issue, which is available at wileyonlinelibrary.com.]

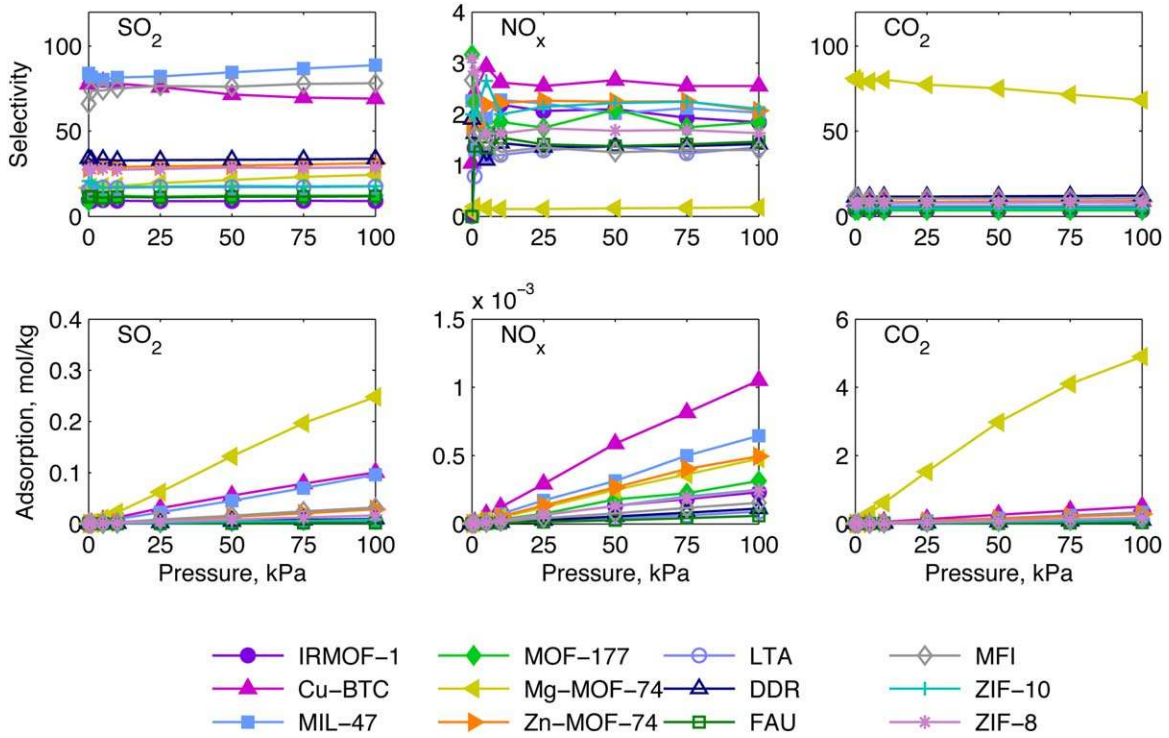

Figure 5. Simulated adsorption loading (q_i) and selectivity (S_{ads}) of SO_2, NO_x, and CO_2 as a function of total pressure in the mixture of N_2—CO_2—O_2—SO_2—NO_2—NO at 313 K in 12 porous materials.

The composition of gas mixture is $N_2/CO_2/O_2/SO_2/NO_2/NO = 0.7975/0.15/0.05/0.002/0.00025/0.00025$ (by volume). [Color figure can be viewed in the online issue, which is available at wileyonlinelibrary.com.]

Interactions between guest molecules and frameworks

Figures 3 and 4 compare the isotherms and the isosteric heats of adsorption of six pure components in all of 12 porous materials. In general, SO_2 has the largest loading at 100 kPa, followed by CO_2, NO_2, and NO. It should be noted that for IRMOF-1 and MOF-177, the loadings of SO_2 show sharp increase as the pressure is above 0.075 MPa, which may indicate the occurrence of condensation.

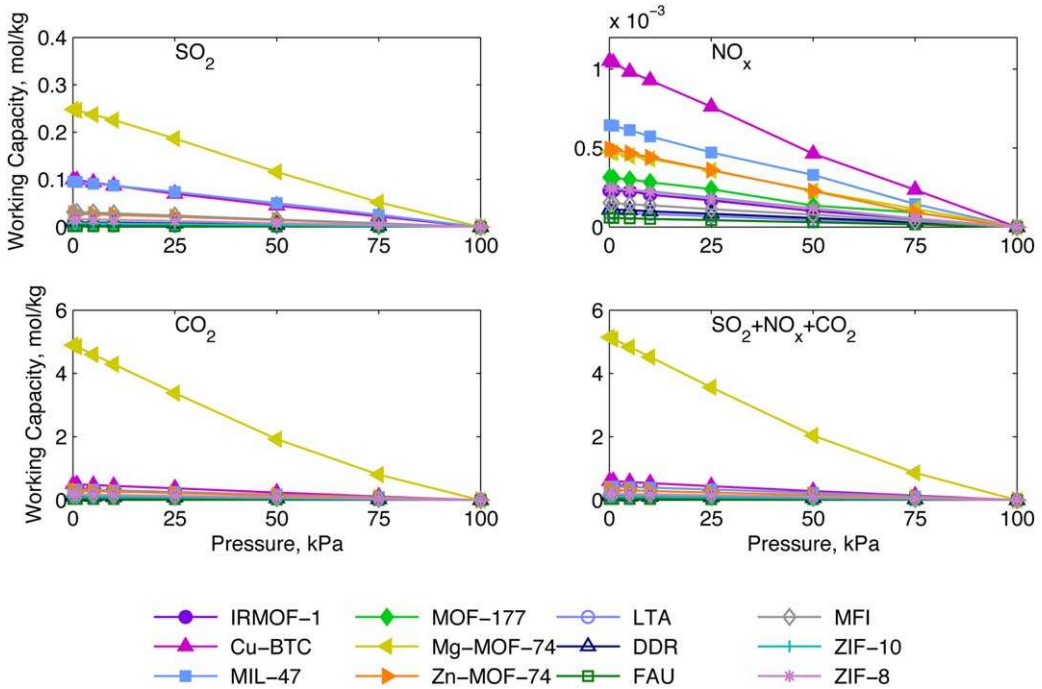

Figure 6. Working capacity (Δq_i) of SO_2, NO_x, and CO_2 as a function of desorption pressure in the mixture of N_2—CO_2—O_2—SO_2—NO_2—NO at 313 K in 12 porous materials given from our simulations.

The adsorption pressure is at 1 bar, and the composition of gas mixture is $N_2/CO_2/O_2/SO_2/NO_2/NO = 0.7975/0.15/0.05/0.002/0.00025/0.00025$ (by volume). [Color figure can be viewed in the online issue, which is available at wileyonlinelibrary.com.]

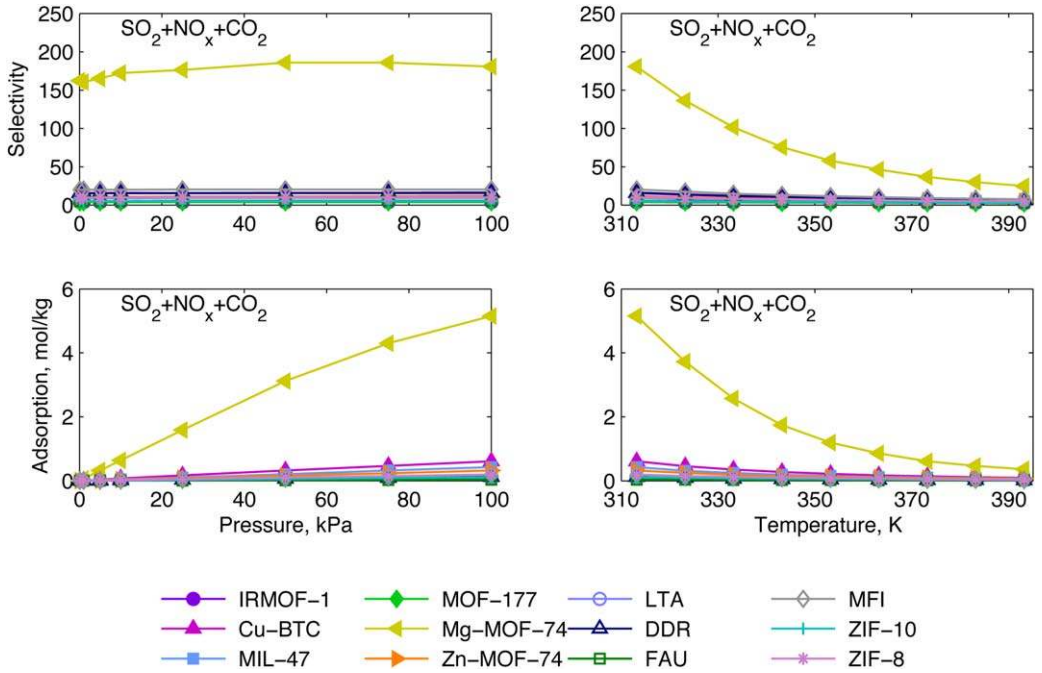

Figure 7. Simulated (upper) adsorption selectivity (S_{ads}) and (lower) absolute adsorption (q_i) as a function of (left) total pressure and (right) temperature for simultaneous removals of SO_2, NO_x, and CO_2 from the flue gases mixture in 12 porous materials.

The composition of gas mixture is $N_2/CO_2/O_2/SO_2/NO_2/NO$ = 0.7975/0.15/0.05/0.002/0.00025/0.00025 (by volume). [Color figure can be viewed in the online issue, which is available at wileyonlinelibrary.com.]

Figure 4 shows that those species with a higher heat of adsorptions have larger uptakes. In particular at low pressures, there is a strong correlation between loading and heat of adsorption. The higher uptakes can be attributed to the stronger binding energy between the guest molecules and frameworks.

Removal of SO_2 from the mixture of N_2—CO_2—O_2—SO_2—NO_2—NO

Figure 5 presents the absolute adsorption and adsorption selectivity of SO_2, NO_x, and CO_2, respectively, in all of these 12 porous materials at the proposed mixture composition as a function of total pressure.

Based on the absolute adsorption shown in Figure 5, the best materials for the removal of SO_2 from the flue gases (N_2—CO_2—O_2—SO_2—NO_2—NO) is Mg-MOF-74, followed by Cu-BTC and MIL-47 among these 12 porous materials. It is expected that Mg-MOF-74 and Cu-BTC have advantages in adsorbing SO_2 given that the unsaturated open-metal sites have a strong affinity with polar molecules such as SO_2. As reported in the literature, for Cu-BTC, the electrostatic interaction between the polar guest molecules and the partial charges on the framework atoms dominates the adsorption mechanism.[62] Interestingly, MIL-47 also shows an excellent adsorption performance in removing SO_2, which might be attributed to the topology of MIL-47. In a recent publication, MIL-47 was recommended as one of the most promising materials for the removal of sulfur dioxide from the flue gases at the pressure of 4 MPa.[6]

Figure 6 presents the working capacity of SO_2, NO_x, and CO_2 in a variety of MOFs and zeolites as a function of pressure. It is believed that more open structures with high pore volumes and high surface areas can potentially yield higher working capacities.[14] Generally speaking, MOFs possess higher pore volumes and surface areas than zeolites. So, it is expected that MOFs have better performance in working capacity than zeolites. For example, from Figure 6, we can see that Mg-MOF-74, Cu-BTC, and MIL-47 are the best materials based on working capacity for the removal of sulfur dioxide.

From the selectivity point of views, we can see from Figure 5 that the best materials for the removal of SO_2 are MIL-47, MFI, and Cu-BTC. It is notable that Mg-MOF-74 is not among the top materials according to the selectivity although it performed the best in terms of the absolute adsorption and working capacity. This can be traced to the large uptake of CO_2 in the flue gas mixture on Mg-MOF-74, which can be explained by the following three points. First, compared with other materials possessing open-metal sites studied in this work, Mg-MOF-74 has the highest density of open-metal sites on the basis of either per unit of surface area or per unit of free volume of frameworks.[15] Next, the larger quadrupole moment and higher polarizability of CO_2 favor its adsorption on the open-metal sites. Finally, the composition of CO_2 in the flue gas is the second largest, and two orders of magnitude higher than SO_2. Accordingly, CO_2 will be more preferentially adsorbed on Mg-MOF-74 than other guest molecules in the flues gas. As a result, the Mg-MOF-74 is not recommended. And also, the zeolite MFI is not promising because of its poor performance in absolute adsorption q_i and poor working capacity Δq_i.

Based on the evaluations of absolute adsorption q_i, adsorption selectivity S_{ads}, and working capacity Δq_i, we suggest that both Cu-BTC and MIL-47 are the most promising materials among the examined ones here for the removal of SO_2 from the flue gases mixture.

Removal of NO_x from the mixture of N_2—CO_2—O_2—SO_2—NO_2—NO

For the removal of another kind of harmful gas nitrides, it can be seen from Figure 5 that the best candidate material is

Cu-BTC on the basis of our three sorting criteria: absolute adsorption, selectivity, and working capacity. However, the results show that both the adsorbed amount and selectivity are up to two orders of magnitudes lower than the performance of these promising materials for removing SO_2. Although NO_2 and NO are also polar molecules, their corresponding dipole moments (i.e., 0.32D and 0.15D, respectively) are much lower than that of SO_2 (i.e., 1.63D).[63] As a result, the interaction between open-metal sites and NO_x is not large enough to provide strong and selective adsorption under this extremely small composition.

Although MIL-47 also has good performance in two sorting criteria such as absolute adsorption q_i and working capacity Δq_i, but it falls behind other adsorbents according to adsorption selectivity S_{ads}. Accordingly, we recommend Cu-BTC as the only one best adsorbent among those examined here for the removal of NO_x from the flue gases mixture.

Simultaneous removal of SO_2, NO_x, and CO_2 from the mixture of N_2—CO_2—O_2—SO_2—NO_2—NO

For the simultaneous removals of SO_2, NO_x, and CO_2 from the flue gases mixture, the biggest absolute total adsorption comes from Mg-MOF-74 (see Figure 7). And, the sorting results based on the working capacity also lead to this adsorbent (see Figure 6). We note that the screening result is as same as the separation of CO_2 from the flue gases presented in Figures 5 and 6. Similarly, the uptakes of CO_2 are large because of its larger quadrupole moment and higher polarizability. In addition, the content of CO_2 in flue gases mixture is as more as 15%, which is more than any other components except N_2. As a result, we recommend Mg-MOF-74 as a promising material among the examined ones here for the simultaneous removal of SO_2, NO_x, and CO_2 from the flue gases mixture.

At this point, it is instructive to point out that the influence of SO_2 and NO_x on the determination of the promising materials for the removal of CO_2 cannot be completely neglected. The presence of trace amount of SO_2 and NO_x could have influence on the adsorption performance, such as adsorption selectivity. Essentially, those adsorbed SO_2 molecules occupied some adsorption sites and made them inaccessible for CO_2. Some researchers have confirmed that compared with a system without SO_2, smaller CO_2/N_2 selectivity was observed for the system of CO_2—NO_2—H_2O—SO_2 over the pressure range of 0.08–0.14 MPa.[37]

Conclusions

As two principal pollutants listed in the U.S. NAAQS, both SO_2 and NO_x are harmful to human health and environment. It is crucial to separate them from flue gases before emitting into the atmosphere. In this present work, 12 porous materials were selected to separate SO_2 and NO_x from gas mixture, including six MOFs, two ZIFs, and four zeolites. Their adsorption performances were evaluated using GCMC molecular simulation technique and three criteria such as absolute adsorption, adsorption selectivity, and working capacity. For the removal of SO_2, both Cu-BTC and MIL-47 performed best and were chosen as the most promising materials. The presence of open-metal sites in Cu-BTC and suitable pore sizes can explain good separation performance of Cu-BTC. Next, Cu-BTC was proved to be the best adsorbent for the removal of NO_x from the flue gases mixture. Due to the small dipole moment of NO_x, all of these materials, however, cannot provide separation with very large capacity and high selectivity. Finally, we further considered the simultaneous removal of SO_2, NO_x, and CO_2 from flue gases. Mg-MOF-74 was recommended as the only potential material for this separation due to its high density of open-metal sites which provides strong interactions with dipole and quadruple molecules.

Acknowledgments

WZS and XP were supported by the China Scholarship Council (CSC). XP was supported by the Open Project of State Key Laboratory of Clean Energy Utilization (No. ZJUCEU2010020), and the Open Project of State Key Laboratory of Chemical Engineering (SKL-Che-12C01). LCL and BS were supported as part of the Center for Gas Separations Relevant to Clean Energy Technologies, an Energy Frontier Research Center funded by the U.S. Department of Energy, Office of Science, Office of Basic Energy Sciences under Award Number DE-SC0001015.

Literature Cited

1. National Ambient Air Quality Standards. 2011. Available at: www.epa.gov/air/criteria.html. Last accessed 2014.
2. Das AK, De Wilde J, Heynderickx GJ, Marin GB, Iversen SB, Felsvang K. Simultaneous adsorption of SO_2-NOx from flue gases in a riser configuration. *AIChE J*. 2001;47:2831–2844.
3. Xu X, Chen C, Qi H, He R, You C, Xiang G. Development of coal combustion pollution control for SO_2 and NO_x in China. *Fuel Process Technol*. 2000;62:153–160.
4. Granite EJ, Pennline HW. Photochemical removal of mercury from flue gas. *Ind Eng Chem Res*. 2002;41:5470–5476.
5. D'Alessandro DM, Smit B, Long JR. Carbon dioxide capture: prospects for new materials. *Angew Chem Int Ed*. 2010;49:6058–6082.
6. Peng X, Cao D. Computational screening of porous carbons, zeolites, and metal organic frameworks for desulfurization and decarburization of biogas, natural gas, and flue gas. *AIChE J*. 2013;59:2928–2942.
7. Srivastava RK, Jozewicz W. Flue gas desulfurization: the state of the art. *J Air Waste Manag Assoc*. 2001;51:1676–1688.
8. Shelef M. Selective catalytic reduction of NOx with N-free reductants. *Chem Rev*. 1995;95:209–225.
9. Gollakota SV, Chriswell CD. Study of an adsorption process using silicalite for sulfur dioxide removal from combustion gases. *Ind Eng Chem Res*. 1988;27:139–143.
10. Yeh JT, Ma WT, Pennline HW, Haslbeck JL, Joubert JI, Gromicko FN. Integrated testing of the NOXSO process: simultaneous removal of SO_2 and NOx from flue gas. *Chem Eng Commun*. 1992;114:65–88.
11. Davini P. SO_2 and NOx adsorption properties of activated carbons obtained from a pitch containing iron derivatives. *Carbon*. 2001;39:2173–2179.
12. Deng H, Yi H, Tang X, Yu Q, Ning P, Yang L. Adsorption equilibrium for sulfur dioxide, nitric oxide, carbon dioxide, nitrogen on 13X and 5A zeolites. *Chem Eng J*. 2012;188:77–85.
13. Zhou H-C, Long JR, Yaghi OM. Introduction to metal-organic frameworks. *Chem Rev*. 2012;112:673–674.
14. Krishna R, van Baten JM. In silico screening of metal-organic frameworks in separation applications. *Phys Chem Chem Phys*. 2011;13:10593–10616.
15. Yazaydin AO, Snurr RQ, Park T-H, Koh K, Liu J, LeVan MD, Benin AI, Jakubczak P, Lanuza M, Galloway DB, Low JJ, Willis RR. Screening of metal-organic frameworks for carbon dioxide capture from flue gas using a combined experimental and modeling approach. *J Am Chem Soc*. 2009;131:18198–18199.
16. Lin L-C, Berger AH, Martin RL, Kim J, Swisher JA, Jariwala K, Rycroft CH, Bhown AS, Deem MW, Haranczyk M, Smit B. In silico screening of carbon-capture materials. *Nat Mater*. 2012;11:633–641.
17. Dzubak AL, Lin L-C, Kim J, Swisher JA, Poloni R, Maximoff SN, Smit B, Gagliardi L. Ab initio carbon capture in open-site metal–organic frameworks. *Nat Chem*. 2012;4:810–816.
18. An J, Rosi NL. Tuning MOF CO_2 adsorption properties via cation exchange. *J Am Chem Soc*. 2010;132:5578–5579.

19. Babarao R, Jiang J. Unprecedentedly high selective adsorption of gas mixtures in rho zeolite-like metal-organic framework: a molecular simulation study. *J Am Chem Soc*. 2009;131:11417–11425.
20. Zhao D, Timmons DJ, Yuan D, Zhou H-C. Tuning the topology and functionality of metal-organic frameworks by ligand design. *Acc Chem Res*. 2011;44:123–133.
21. Bae Y-S, Farha OK, Hupp JT, Snurr RQ. Enhancement of CO_2/N_2 selectivity in a metal-organic framework by cavity modification. *J Mater Chem*. 2009;19:2131–2134.
22. Herm ZR, Swisher JA, Smit B, Krishna R, Long JR. Metal-organic frameworks as adsorbents for hydrogen purification and precombustion carbon dioxide capture. *J Am Chem Soc*. 2011;133:5664–5667.
23. Smit B, Maesen TLM. Molecular simulations of zeolites: adsorption, diffusion, and shape selectivity. *Chem Rev*. 2008;108:4125–4184.
24. Park KS, Ni Z, Côté AP, Choi JY, Huang R, Uribe-Romo FJ, Chae HK, O'Keeffe M, Yaghi OM. Exceptional chemical and thermal stability of zeolitic imidazolate frameworks. *Proc Natl Acad Sci USA*. 2006;103:10186–10191.
25. Chen B, Ockwig NW, Millward AR, Contreras DS, Yaghi OM. High H_2 adsorption in a microporous metal-organic framework with open metal sites. *Angew Chem Int Ed*. 2005;44:4745–4749.
26. Baerlocher C, McCusker LB. Database of Zeolite Structures. 2013. Available at: http://www.iza-structure.org/databases/. Last accessed 2014.
27. Jakobtorweihen S, Hansen N, Keil FJ. Combining reactive and configurational-bias Monte Carlo: confinement influence on the propene metathesis reaction system in various zeolites. *J Chem Phys*. 2006;125:224709.
28. Eddaoudi M, Kim J, Rosi N, Vodak D, Wachter J, O'Keeffe M, Yaghi OM. Systematic design of pore size and functionality in isoreticular MOFs and their application in methane storage. *Science*. 2002;295:469–472.
29. Chui SS. A chemically functionalizable nanoporous material $[Cu_3(TMA)_2(H_2O)_3]$n. *Science*. 1999;283:1148–1150.
30. Vishnyakov A, Ravikovitch PI, Neimark AV, Bülow M, Wang QM. Nanopore structure and sorption properties of Cu-BTC metal-organic framework. *Nano Lett*. 2003;3:713–718.
31. Barthelet K, Marrot J, Riou D, Férey G. A breathing hybrid organic–inorganic solid with very large pores and high magnetic characteristics. *Angew Chem Int Ed Engl*. 2002;41:281–284.
32. Chae HK, Siberio-Pérez DY, Kim J, Go YB, Eddaoudi M, Matzger AJ, O'Keeffe M, Yaghi OM. A route to high surface area, porosity and inclusion of large molecules in crystals. *Nature*. 2004;427:523–527.
33. Grant Glover T, Peterson GW, Schindler BJ, Britt D, Yaghi O. MOF-74 building unit has a direct impact on toxic gas adsorption. *Chem Eng Sci*. 2011;66:163–170.
34. Rosi NL, Kim J, Eddaoudi M, Chen B, O'Keeffe M, Yaghi OM. Rod packings and metal-organic frameworks constructed from rod-shaped secondary building units. *J Am Chem Soc*. 2005;127:1504–1518.
35. Banerjee R, Phan A, Wang B, Knobler C, Furukawa H, O'Keeffe M, Yaghi OM. High-throughput synthesis of zeolitic imidazolate frameworks and application to CO_2 capture. *Science*. 2008;319:939–943.
36. Potoff J, Siepmann J. Vapor–liquid equilibria of mixtures containing alkanes, carbon dioxide, and nitrogen. *AIChE J*. 2001;47:1676–1682.
37. Yu J, Ma Y, Balbuena PB. Evaluation of the impact of H_2O, O_2, and SO_2 on postcombustion CO_2 capture in metal-organic frameworks. *Langmuir*. 2012;28:8064–8071.
38. Sokolic F, Guissani Y, Guillot B. Molecular dynamics simulations of thermodynamic and structural properties of liquid SO_2. *Mol Phys*. 1985;56:239–253.
39. Bourasseau E, Lachet V, Desbiens N, Maillet J-B, Teuler J-M, Ungerer P. Thermodynamic behavior of the $CO_2 + NO_2/N_2O_4$ mixture: a Monte Carlo simulation study. *J Phys Chem B*. 2008;112:15783–15792.
40. Zhou Z, Todd BD, Travis KP, Sadus RJ. A molecular dynamics study of nitric oxide in water: diffusion and structure. *J Chem Phys*. 2005;123:054505.
41. Liu B, Smit B. Comparative molecular simulation study of CO_2/N_2 and CH_4/N_2 separation in zeolites and metal-organic frameworks. *Langmuir*. 2009;25:5918–5926.
42. García-Pérez E, Parra JB, Ania CO, García-Sánchez A, Van Baten JM, Krishna R, Dubbeldam D, Calero S. A computational study of CO_2, N_2, and CH_4 adsorption in zeolites. *Adsorption*. 2007;13:469–476.
43. Martín-Calvo A, García-Pérez E, Manuel Castillo J, Calero S. Molecular simulations for adsorption and separation of natural gas in IRMOF-1 and Cu-BTC metal-organic frameworks. *Phys Chem Chem Phys*. 2008;10:7085–7091.
44. Walton KS, Millward AR, Dubbeldam D, Frost H, Low JJ, Yaghi OM, Snurr RQ. Understanding inflections and steps in carbon dioxide adsorption isotherms in metal-organic frameworks. *J Am Chem Soc*. 2008;130:406–407.
45. Dubbeldam D, Frost H, Walton KS, Snurr RQ. Molecular simulation of adsorption sites of light gases in the metal-organic framework IRMOF-1. *Fluid Phase Equilib*. 2007;261:152–161.
46. Rosenbach N, Jobic H, Ghoufi A, Salles F, Maurin G, Bourrelly S, Llewellyn PL, Devic T, Serre C, Férey G. Quasi-elastic neutron scattering and molecular dynamics study of methane diffusion in metal organic frameworks MIL-47(V) and MIL-53(Cr). *Angew Chem Int Ed Engl*. 2008;47:6611–6615.
47. Keskin S. Atomistic simulations for adsorption, diffusion, and separation of gas mixtures in zeolite imidazolate frameworks. *J Phys Chem C*. 2011;115:800–807.
48. Zhou M, Wang Q, Zhang L, Liu Y-C, Kang Y. Adsorption sites of hydrogen in zeolitic imidazolate frameworks. *J Phys Chem B*. 2009;113:11049–11053.
49. Xu Q, Zhong C. A general approach for estimating framework charges in metal−organic frameworks. *J Phys Chem C*. 2010;114:5035–5042.
50. Rappe A, Casewit C, Colwell K, Goddard W III, Skiff W. UFF, a full periodic table force field for molecular mechanics and molecular dynamics simulations. *J Am Chem Soc*. 1992;114:10024–10035.
51. Yang Q, Zhong C, Chen J-F. Computational study of CO_2 storage in metal-organic frameworks. *J Phys Chem C*. 2008;112:1562–1569.
52. Zheng C, Liu D, Yang Q, Zhong C, Mi J. Computational study on the influences of framework charges on CO_2 uptake in metal-organic frameworks. *Ind Eng Chem Res*. 2009;48:10479–10484.
53. Lin L-C, Lee K, Gagliardi L, Neaton JB, Smit B. Force-field development from electronic structure calculations with periodic boundary conditions: applications to gaseous adsorption and transport in metal-organic frameworks. *J Chem Theory Comput*. 2014;10:1477–1488.
54. Frenkel D, Smit B. *Understanding Molecular Simulation: From Algorithms to Applications*, 2nd ed. San Diego: Academic Press, 2002.
55. Swisher JA, Lin L-C, Kim J, Smit B. Evaluating mixture adsorption models using molecular simulation. *AIChE J*. 2013;59:22–24.
56. Mason JA, Sumida K, Herm ZR, Krishna R, Long JR. Evaluating metal-organic frameworks for post-combustion carbon dioxide capture via temperature swing adsorption. *Energy Environ Sci*. 2011;4:3030–3040.
57. Saha D, Bao Z, Jia F, Deng S. Adsorption of CO_2, CH_4, N_2O, and N_2 on MOF-5, MOF-177, and zeolite 5A. *Environ Sci Technol*. 2010;44:1820–1826.
58. Millward AR, Yaghi OM. Metal-organic frameworks with exceptionally high capacity for storage of carbon dioxide at room temperature. *J Am Chem Soc*. 2005;127:17998–17999.
59. Zhu W, Hrabanek P, Gora L, Kapteijn F, Moulijn JA. Role of adsorption in the permeation of CH_4 and CO_2 through a silicalite-1 membrane. *Ind Eng Chem Res*. 2006;45:767–776.
60. Himeno S, Tomita T, Suzuki K, Yoshida S. Characterization and selectivity for methane and carbon dioxide adsorption on the all-silica DD3R zeolite. *Microporous Mesoporous Mater*. 2007;98:62–69.
61. Cavenati S, Grande CA, Rodrigues AE. Metal organic framework adsorbent for biogas upgrading. *Ind Eng Chem Res*. 2008;47:6333–6335.
62. Karra JR, Walton KS. Effect of open metal sites on adsorption of polar and nonpolar molecules in metal-organic framework Cu-BTC. *Langmuir*. 2008;24:8620–8626.
63. Nelson RDJ, Lide DRJ, Maryott AA. *Selected Values of Electric Dipole Moments for Molecules in the Gas Phase*. Washington, D.C.: U.S. National Bureau of Standards, 1967.

Manuscript received Dec. 4, 2013, and revision received Mar. 20, 2014.